Speleothem biomarker evidence for a negative terrestrial feedback on climate during Holocene warm periods

Wang, Canfa; Bendle, James; Greene, Sarah; Griffiths, Michael L.; Huang, Junhua; Moossen, Heiko; Zhang, Hongbin ; Ashley, Kate; Xie, Shucheng

DOI:
10.1016/j.epsl.2019.115754

Highlights

- The first compound specific $\delta^{13}C$ analysis of fatty acids from a stalagmite
- Proportional increases in C_3 plants during warmer/wetter Holocene intervals
- Soil respiration is more substrate selective during warmer/wetter Holocene intervals
- Primary production outpaces soil respiration during warmer/wetter Holocene intervals
- Subtropical mineral soils act as a negative feedback in a warmer/wetter climate

Speleothem Biomarker Evidence for a Negative Terrestrial Feedback on Climate During Holocene Warm Periods

Canfa Wang[a,b], James A. Bendle[b], Sarah E. Greene[b], Michael L. Griffiths[c], Junhua Huang[d], Heiko Moossen[b], Hongbin Zhang[a], Kate Ashley[b], Shucheng Xie[a*]

[a] State Key Laboratory of Biogeology and Environmental Geology, Hubei Key Laboratory of Critical Zone Evolution, School of Earth Sciences, China University of Geosciences, Wuhan, 430074, China

[b] School of Geography, Earth and Environmental Sciences, University of Birmingham, Birmingham, B15 2TT, UK

[c] Department of Environmental Science, William Paterson University, Wayne, NJ 07470, USA

[d] State Key Laboratory of Geological Processes and Mineral Resources, China University of Geosciences, Wuhan, 430074, China

[*] Corresponding author. Tel: +862767883001 Fax: +862767883002 E-mail address: xiecug@163.com (S. Xie).

Abstract

Understanding how terrestrial carbon storage feeds back on warm climate states is critical for improving global warming projections. Soils may act as a positive feedback on climate if warming increases soil carbon decomposition rates. Conversely, if increases in net primary production (NPP) exceed increases in decomposition, the climate feedback will be negative. Here we utilize the first palaeoclimatic application of compound-specific $\delta^{13}C$ measurements on *n*-fatty acid biomarkers (extracted from a stalagmite from central China) to constrain the response of catchment terrestrial carbon cycle feedbacks during warmer phases of the Holocene. We resolve proportional increases in C_3 plants in the catchment area during these warmer/wetter intervals. Moreover, we infer that heterotrophic soil respiration was highly substrate selective, indicating that NPP outpaced decomposition and the catchment behaved as a carbon sink (mediated and enhanced by changes in the relative proportion of C_3 vs C_4 plants). Thus, we provide palaeoclimate evidence that subtropical soils in a warmer/wetter climate acted as a sink for organic carbon, and thus as a negative climate feedback, during warmer climatic phases.

Keywords

Speleothem; Fatty acids; Carbon isotope; Vegetation; Soil respiration; Negative feedback

1. Introduction

Constraining the effect of climate change on terrestrial respiration and associated feedbacks is critical to furthering our understanding of the global carbon cycle (Mahecha et al., 2010). Globally, soil respiration contributes ca. 100 PgC/yr from the soil to the atmosphere and is sensitive to changes in temperature and precipitation (Bond-Lamberty and Thomson, 2010). If warming increases decomposition rates and transfers carbon stored belowground to the atmosphere, a positive feedback to climate change will occur. Conversely, if increases of plant-derived carbon inputs to soils exceed increases in decomposition, the feedback will be negative. Laboratory and mesocosm experiments to interrogate the response of soil carbon to climate change show highly variable results (see review by Davidson and Janssens (2006) and refs therein). Moreover, laboratory and mesocosm experiments have limited ecosystem complexity and operate on limited timescales, from years to decades (Melillo et al., 2017). Thus, the longer-term climate sensitivity of soil organic matter and global soil carbon stocks, at the whole ecosystem level, is still subject to debate (Davidson and Janssens, 2006). An alternative to laboratory and mesocosm studies is to use palaeoclimate data, which inherently incorporates the response of the whole system. A recent ice-core based study used centennial scale data to derive an estimate for the response of gross primary production and ecosystem respiration to cold climate state during the Little Ice Age cooling (LIA) (Rubino et al., 2016). However, the sensitivity of ecosystem respiration to past warm climate states has not yet been investigated as we lack geological proxies to quantify net primary production and terrestrial respiration. Constraining the intensity of feedback mechanisms between terrestrial ecosystems and warmer climates, on longer timescales, and in natural settings, is central to understanding the global carbon cycle, and thus a prerequisite for reliable future climate projections.

Speleothems are versatile terrestrial archives of palaeoclimate because they have the ability to record changes in ambient environmental conditions at the time of deposition, and can preserve

material transported from overlying ecosystems via karst drip waters (Fairchild and Baker, 2012). *Normal (n-)* alkyl lipid biomarkers are produced by higher plants, algae, and bacteria, and are preserved in various palaeoclimate archives. In speleothems, however, *n*-alkyls have the potential to constrain these ambiguities and isolate catchment vegetation and bacterial changes. The $\delta^{13}C$ of high molecular weight *n*-alkyls (leaf waxes predominantly produced by higher plants) preserved in lake (Huang et al., 2001) and marine (Hughen et al., 2004) sediments, along with palaeosols (Zhang et al., 2006), has been used extensively to reconstruct changes in the relative abundance of C_3 vs C_4 plants. Low molecular weight *n*-alkyl $\delta^{13}C$ records are typically overlooked in palaeoclimate archives because they are produced by three end-members (plants, algae, and bacteria), rendering interpretation challenging. In speleothems though, algal contributions are likely minimal (Fairchild and Baker, 2012), meaning that low molecular weight *n*-alkyls derive from a simpler two end-member system, produced by higher plants and bacteria. Therefore, the compound-specific records of $\delta^{13}C$ entrapped in the calcite can be more directly linked to sources and processes (e.g. bacterial respiration, catchment vegetation, etc.) (Blyth et al., 2016), something which cannot, for example, be achieved from the carbon isotope compositions of bulk calcite (Fairchild and Baker, 2012; Genty et al., 2003), operationally defined organic matter (e.g. acid-soluble organic matter (ASOM) (Li et al., 2014), or non-purgeable organic carbon (NPOC) (Blyth et al., 2013)). Hence, the $\delta^{13}C$ of lipid biomarkers in speleothems represents a uniquely direct line of evidence for vegetation and bacterial changes in terrestrial ecosystems.

Here we present the first record of soil bacterial respiration (a critical component of terrestrial ecosystem respiration) and vegetation changes from central East Asia using compound-specific carbon isotopes extracted from a cave speleothem covering the past 9,000 years. Our novel record is based on the $\delta^{13}C$ of low molecular weight (LMW; $\leq C_{20}$) and high molecular weight (HMW; $>C_{20}$) *n*-fatty acids (a subset of *n*-alkyls) from a previously-reported Holocene speleothem (HS4) recovered from Heshang Cave (Hu et al., 2008b) (Fig. 1), located in

the East Asian monsoon region of central China (Wang et al., 2018). The temperature and hydrological conditions in this region have been reconstructed by multiple proxies from the HS4 stalagmite (Wang et al., 2016; Wang et al., 2018; Xie et al., 2013; Zhu et al., 2017). The 3-hydroxy fatty acid (3-OH-FA) biomarker based RAN_{15} proxy reconstructs mean annual temperature variations of ca.16 to 21°C during the last 9 ka BP, with a relatively warm period in the early to middle Holocene (8.0–6.0 ka BP), and then a relatively cool period in the late Holocene (Wang et al., 2018) (see Fig. 5d). The hydrological conditions for the region have also been reconstructed from multiple archives and proxies, including the 3-OH-FA biomarker-based RIAN proxy from the HS4 stalagmite (Fig. 5g), which, for the Holocene, indicate two relatively long wet periods and one relatively dry period, 8.8–5.9 ka BP, 3.0–0 ka BP and 5.9–3.0 ka BP respectively (Wang et al., 2018; Xie et al., 2013; Zhu et al., 2017). In this current study we demonstrate a marked increase in C_3 vegetation during warm periods of the Holocene epoch, namely the Holocene Climate Optimum (HCO; ca. 4.4 to 8.8 ka BP) and Medieval Warm Period (MWP). Moreover, a deconvolved record of soil bacterial respiration and substrate selectivity implies that the catchment behaved as a net carbon sink during these warm intervals, thus acting as a negative climate feedback.

2. Materials and Methods

2.1 Study site and sample information

Heshang Cave is located at 294m above sea level (a.s.l.), in the Qing River, a tributary in the middle reaches of the Yangtze River, central China (30°27′N, 110°25′E). Heshang Cave is a dissolutional cave system formed in Cambrian dolomite, the overlying dolomite is ca. 400 m thick and is capped with a mature layer of soil (20-40 cm-thick) and reasonably dense vegetation (Hu et al., 2008a). The regional climate is strongly impacted by the East Asian Monsoon, with a hot and moist summer, but relatively cold and dry winter (An, 2000). The average annual precipitation in this region is 1161 mm, based on the recent 64 years (1951-2014) of

meteorological data from Yichang station (located ca.100 km east of Heshang Cave). The seasonal temperature ranges, inside and immediately outside the cave, were constrained by 2-h resolution logging between 2003 - 2007 using HOBO H8 Pro T loggers (Hu et al., 2008a). The modern temperature immediately outside the cave varies seasonally from 3°C to 30°C, with an annual average of 18°C and is statistically identical to that of the nearest government meteorological station at Changyang county (Hu et al., 2008a).

The HS4 stalagmite is 2.5 m long, and was actively growing when collected from ca. 150 m within Heshang Cave in 2001. Soil samples were collected in 2013 from the thin soil layers overlying Heshang Cave, more details were reported in Wang et al. (2018). A detailed description of the age model of HS4 stalagmite can be found in Hu et al. (2008b).

2.2 Lipid Extraction and Work-Up

In order to prevent external contamination during the experiments, all the glassware was first soaked overnight in a decontamination solution, then rinsed in deionised water, dried and combusted for 6h at 500°C. All solvents were purchased at the highest purity available (Absolv, TEDIA) and were checked for purity using gas chromatography–mass spectrometry prior to use. The HCl was pre-extracted with dichloromethane (DCM, ×4), and all other reagents were tested for background contaminants.

The stalagmite samples were treated with an optimized acid digestion method following Wang et al. (2012). In brief, 10 grams of stalagmite sample were digested with 3M HCl, then re-fluxed at 130°C for 3 hours with a condenser/ electrothermal heating mantle assembly. An internal standard (pregn-5-en-3.belta.-ol) was quantitatively added to each sample to quantify the amount of lipids in the stalagmite. After cooling, the residue was extracted by dichloromethane (15mL×4) and the extracts combined. Solvents were removed by rotary evaporation (Buchi R210) under reduced pressure.

The condensed lipids were further derivatized by BF_3-methanol (14% BF_3/methanol, Sigma) before undergoing column separation. The elute solvent are successively in Hexane, Hexane:DCM (2:1, v/v), DCM and Methanol. The fatty acid methyl esters are in the DCM eluted fraction.

2.3 Instrumental Analysis

Identification of *n*-alkanoic acids was performed on an Agilent 7890B gas chromatograph (GC) coupled to an Agilent 5977A mass spectrometer (MS) using a BPI fused silica capillary column (60 m×0.25 mm id.; 0.25 μm film thickness). The GC oven temperature was programmed from 70°C to 130°C at 10°C per min, then from 130°C to 340°C at 3°C per min, and finally held at 340°C for 10 min. The carrier gas was Helium (2.7 mL/min). The MS was operated in electron-impact (EI) mode, the ionization energy was set at 70 eV and the scan range was from 50 to 550 aum.

All the stalagmite samples were quantified on an Agilent 7890B gas chromatograph-FID detector for quantification, separation was performed on a BPI fused silica capillary column (60 m×0.25 mm id.; 0.25 μm film thickness). The GC oven temperature was programmed from 70°C (1min) to 150°C ramped at 30°C per min, then from 150°C to 340°C at 3°C per min, and finally held at 340°C for 10 min.

Compound-specific $\delta^{13}C$ analyses of the C_{16}, C_{18}, C_{22}, C_{24} *n*-fatty acids were performed on an Agilent 7890A GC coupled to an Isoprime GC5 furnace and an IsoPrime100 isotope ratio mass spectrometer. The Isoprime GC5 contains a CuO furnace tube and is kept at 850°C. The GC was equipped with a 60 m BPI column (SGE) (i.d. = 0.25 mm, film thickness = 0.25 μm), with helium as the carrier gas, set at a constant flow of 1.7 ml/min, the oven was programmed from 70°C (1 min) to 150°C ramped at 30°C /min, then from 150°C to 340°C at 3°C per min, and finally held at 340°C for 5 min.

160 The carbon isotope values are reported as per mil (‰) deviations from Vienna Pee Dee
161 Belemnite (VPDB) in standard delta notation. A homemade mixture of *n*-alkanes standard and an
162 authenticated standard *n*-fatty acid methyl and ethyl esters mixture with known $\delta^{13}C$ (F8; Arndt
163 Schimmelmann, Indiana University) were measured regularly between a maximum of 5 sample
164 injections to test the conditions of the instrument and determine the $\delta^{13}C$ values of the *n*-alkanoic
165 acids. Each sample was run at least in duplicate.

166 Correcting the derivatisation effect on $\delta^{13}C$ isotopic signature of the fatty acids was done
167 following Polissar and D'Andrea (2014). The determination of the $\delta^{13}C$ of the methanol is
168 calibrated by a phthalic acid standard with a known $\delta^{13}C$ value bought from A. Schimmelmann,
169 Indiana University.

170

171 *2.4 Calculation of carbon isotopic values of fatty acids derived from bacteria*

172 We isolate the bacterial contribution to the *n*-C_{18} chain length fatty acid, because this chain
173 length is known to be produced by higher plants in low relative abundances (Chikaraishi and
174 Naraoka, 2007; Chikaraishi et al., 2004a; Liu and Liu, 2017; Wang and Liu, 2012). Equation (1)
175 describes the measured $\delta^{13}C_{18FA}$ as a function of the higher plant and bacterial *n*-C_{18} chain length
176 fatty acid carbon isotopic composition ($\delta^{13}C_{18FA(P)}$ and $\delta^{13}C_{18FA(B)}$, respectively) and F, the
177 fractional contribution of higher plants to $\delta^{13}C_{18FA}$.

178 $$\delta^{13}C_{18FA} = F * \delta^{13}C_{18FA(P)} + (1 - F) * \delta^{13}C_{18FA(B)} \quad (1)$$

179 Higher plants do not fractionate differentially during the production of fatty acids within
180 even or odd chain lengths (Chikaraishi and Naraoka, 2007). Therefore, if we presume that
181 exclusively plant-derived $\delta^{13}C_{24FA}$ and the higher plant-derived contribution to $\delta^{13}C_{18FA}$ ($\delta^{13}C_{18FA(P)}$)
182 derived from predominantly the same higher-plant sources in the catchment, then $\delta^{13}C_{24FA}$ and
183 $\delta^{13}C_{18FA(P)}$ should have the same carbon isotopic signature (Chikaraishi and Naraoka, 2007).
184 Rearranging and substituting $\delta^{13}C_{24FA}$ into equation (1) gives us equation (2), which expresses the
185 carbon isotopic signature of the bacterial fraction of C_{18FA} ($\delta^{13}C_{18FA(B)}$) as a function of measured

$\delta^{13}C_{18FA}$, measured $\delta^{13}C_{24FA}$, and F.

$$\delta^{13}C_{18FA(B)} = (\delta^{13}C_{18FA} - F * \delta^{13}C_{24FA}) / (1 - F) \quad (2)$$

F, the fractional contribution of higher plants $\delta^{13}C_{18FA}$, can be expressed as the quotient of the relative abundance of higher plant-derived *n*-C_{18} chain length fatty acids ($C_{18FA(P)}$) divided by the relative abundance of C_{18} chain length fatty acids (C_{18FA}) in each sample:

$$F = C_{18FA(P)}/C_{18FA} \quad (3)$$

We do not know the relative abundance of higher plant-derived C_{18FA} ($C_{18(P)}$) *a priori*, but we can estimate this using the mean ratio of C_{18FA}:C_{24FA} (R) produced by higher plants. The mean R value is 1.14 for the compiled global dataset (see Supplementary Datasheet 1) (Chikaraishi et al., 2004a; Liu and Liu, 2017; Wang and Liu, 2012). Thus, in equation (4) we express $C_{18FA(P)}$ as the product of R and the measured relative abundance of C_{24FA}.

$$C_{18FA(P)} = R * C_{24FA} \quad (4)$$

Combining equations (2), (3), & (4) gives equation (5), which expresses the bacterial carbon isotope signature of each sample ($\delta^{13}C_{18FA(B)}$) as a function of the sampled relative abundances of C_{18FA} and C_{24FA}, the mean C_{18FA}:C_{24FA} ratio of higher plants (R), and the measured carbon isotopic signatures of the C_{18} and C_{24} chain length fatty acids in the sample.

$$\delta^{13}C_{18FA(B)} = (\delta^{13}C_{18FA} - (R * C_{24FA} /C_{18FA})\delta^{13}C_{24FA}) / (1 - R * C_{24FA}/C_{18FA}) \quad (5)$$

The uncertainty in the calculated $\delta^{13}C_{18FA(B)}$ is propagated from the uncertainties of $\delta^{13}C_{18FA}$ and $\delta^{13}C_{24FA}$ according to equation (2). Since there is considerable variability in reported global R values in the literature (Supplementary Datasheet 1), putting an error estimate on this would be highly speculative (and perhaps much too conservative, given that we are operating in a single catchment where the spatial and temporal variability is unlikely to approach the global spread in reported R values. Future research efforts for better constraints on the value of R and soil bacterial biomarkers are needed with the ultimate goal of producing more quantitative estimates of palaeo-respiration). Thus the propagated error is calculated according equation (6) shown below:

$$\delta(\delta^{13}C_{18FA(B)}) = \sqrt{\left(\frac{1}{1-F}\delta a\right)^2 + \left(\frac{F}{1-F}\delta b\right)^2} \quad (6)$$

where δa represents the uncertainty of $\delta^{13}C_{18FA}$, δb represents the uncertainty of $\delta^{13}C_{24FA}$.

Our $\delta^{13}C_{18FA(B)}$ curve is derived by subtracting the $C_{18FA(P)}$ contribution from the C_{18FA} record (e.g. correcting for the direct contribution of higher plants to the C_{18FA}). As a data exploration exercise, we further subtracted the $\delta^{13}C_{24FA(P)}$ record from the $\delta^{13}C_{18FA(B)}$ (see Figure S1). An argument for this approach is that the resultant $\Delta\delta^{13}C_{18FA(B)\text{ - }24FA}$ is a more constrained record of soil bacterial respiration—by doing this, one is attempting to remove the influence of changes in C_3/C_4 vegetation on the bacterial substrate pool. However, calculating $\Delta\delta^{13}C_{18FA(B)\text{ - }24FA}$ entails a two-step subtraction in which a (weighted) $\delta^{13}C_{24FA(P)}$ is added to itself (less $\delta^{13}C_{18FA}$). Given the much larger isotopic range for the $\delta^{13}C_{24FA(P)}$ record compared with the raw $\delta^{13}C_{18FA}$ record, the end result is simply to produce a curve that largely resembles the original $\delta^{13}C_{24FA(P)}$ record with amplified variability. In light of this, we restrict our discussion and interpretation to our $\delta^{13}C_{18FA(B)}$ record.

3. Results and Discussion

3.1 Composition and distribution of fatty acids

The chain length of fatty acids ranges from C_{12} to C_{32} in the overlying soils and from C_{12} to C_{28} in the HS4 stalagmite. In all the sample sets, fatty acids exhibit a bimodal distribution, with a strong predominance of even-carbon-numbered homologues maximizing at *n*-C_{16} and *n*-C_{24}. Trace amounts of branched and monounsaturated fatty acids were found along with the abundant *n*-fatty acids in both the overlying soils and HS4 stalagmite. However, in this study, HMW branched fatty acids were only detected in the HS4 stalagmite (Fig. 2 and Supplementary Datasheet 1), the absence of HMW branched fatty acids in the overlying soils may indicate a contribution of HMW branched fatty acids to the HS4 stalagmite from microorganisms living in the karst or cave environment (Matsumoto et al., 1992). The bimodal distribution pattern of fatty acids in the HS4

stalagmite is the same as the distribution pattern from the same stalagmite reported by Huang et al. (2008) and a stalagmite from a British cave (Blyth et al., 2011), all of which show a dominant carbon maximizing at *n*-C_{16} in the LWM homologues and at *n*-C_{24} in the HMW homologues. The bimodal distribution pattern of fatty acids is similar to that of *n*-alkanes and fatty alcohols which indicates a mixed origin from higher plants and microbes (Xie et al., 2003). We did not detect long chain *n*-fatty acids from C_{29} to C_{32} in the stalagmite samples, suggesting either low concentrations below the detection limit or that they were totally absent. The bimodal distribution of *n*-fatty acids in the HS4 stalagmite is akin to that in the overlying soils, suggesting both share a similar source of fatty acids. The implication is that the *n*-fatty acids in HS4 are dominantly sourced from the overlying soil, with a minor contribution of microbes from inside the karst/cave system, as suggested by the minor component of branched homologues (see discussion in Section 3.3 below).

The percentage of low molecular weight (LMW, $\leq C_{20}$) fatty acids we measured is significantly higher than high molecular weight (HMW, $>C_{20}$) fatty acids. The LMW fatty acids show a similar pattern in the overlying soils and the HS4 stalagmite. The dominant compound *n*-C_{16} fatty acid occupied ca. 35% of the total fatty acids in both the soils and stalagmite samples. The *n*-C_{18} fatty acid is slightly higher in the HS4 stalagmite (ca. 15%) than that of in the overlying soils (ca. 6%) (Fig. 2a, c). HMW fatty acids from cave overlying soils are mainly dominated by *n*-fatty acids with non-detected branched fatty acids, however, trace amount of *iso*- (*i*-) and *anteiso*- (*a*-) fatty acids were found in the HS4 stalagmite accounting for an average around 1% of all fatty acids. The most abundant HMW fatty acid *n*-C_{24} accounted for an average of ca. 7.5% in cave overlying soils and ca. 5.5% in the HS4 stalagmite (Fig. 2b, d).

3.2 Carbon isotopic compositions of fatty acids

We analysed the $\delta^{13}C$ values of the major *n*-fatty acids with 16, 18, 22 and 24 carbon atoms

from the HS4 stalagmite subsamples. The $\delta^{13}C$ of the *n*-C_{16} fatty acid ($\delta^{13}C_{16FA}$) varies from -27.5‰ to -25.2‰. The *n*-C_{18} fatty acid ($\delta^{13}C_{18FA}$) varies from -27.0‰ to -23.4‰, and is slightly enriched in ^{13}C across the whole time series (Fig. 6a). The *n*-C_{22} and *n*-C_{24} fatty acid are relatively more depleted in ^{13}C than the short chain fatty acids *n*-C_{16} and *n*-C_{18}, with $\delta^{13}C_{22FA}$ varying from -32.9‰ to -25.7‰ and $\delta^{13}C_{24FA}$ varying from -33.5‰ to -25.2‰ over the past 8.8 ka BP (Figs. 4, 6a). The variation of $\delta^{13}C_{16FA}$ and $\delta^{13}C_{18FA}$ show a generally parallel trend over the past 8.8 ka BP (R^2 = 0.79, n = 70; Fig. 3a), while the correlation between the HS4 $\delta^{13}C_{16FA}$ and $\delta^{13}C_{24FA}$ is much weaker (R^2 = 0.55, n = 61; Fig. 3b). In addition, the $\delta^{13}C_{22FA}$ and $\delta^{13}C_{24FA}$ are very strongly correlated within the available data set (R^2 = 0.94, n = 49; Fig. 3c), while the correlation between the HS4 $\delta^{13}C_{18FA}$ and $\delta^{13}C_{24FA}$ is much weaker (R^2 = 0.61, n = 59; Fig. 3d). The ^{13}C values of all the analysed *n*-fatty acids from 8.8 to 4.4 ka BP and 0.8 to 0.6 ka BP are more negative than those from 4.4 to 0.8 ka BP and 0.6 to 0 ka BP (Figs. 4, 6a,). Overall, the $\delta^{13}C_{16FA}$ and $\delta^{13}C_{18FA}$ values are relatively positive and vary within a smaller range than that of $\delta^{13}C_{22FA}$ and $\delta^{13}C_{24FA}$ (Fig. 6a).

3.3 Sources of fatty acids in the HS4 stalagmite

We have compared the average distributions of fatty acids within the soils above Heshang Cave (n = 9) to those from HS4 (n = 73) (Fig. 2 and Supplementary Datasheet 1). Strong similarities in distributions between the soil and cave interior suggest that the *n*-fatty acids are primarily sourced from microbes and higher plants living above the cave and/or within the groundwater system, with some minor *in-situ* contribution stalagmite microbrial community possible (Wang et al., 2018). This inference is supported by previous work which concluded that the broad similarity of 3-OH-FA lipid distributions in the overlying soils and stalagmites and the site-specific bacterial 16S rRNA analyses of bacterial diversity and transport pathways (Liu et al., 2010; Yun et al., 2016), demonstrated a major contribution of lipid biomarkers from Gram-negative bacteria dwelling in the overlying soils to the HS4 stalagmite samples.

Furthermore, the 16S rRNA analyses demonstrated that changes in the Gram-negative bacterial community were rapidly transmitted through the Heshang Cave system to drip waters and to the cave and speleothems on seasonal timescales (Yun et al., 2016). Such seasonal responsiveness suggests minimal attenuation of climate signals transmitted from the overlying soils to the HS4 stalagmite (at least sufficient for centennial to millennial scale paleoclimate studies) (Wang et al., 2018). Furthermore, quantitative PCR from Heshang Cave weathered rock yields bacterial 16S rRNA gene abundances of about 10^8 to 10^9 copies g^{-1} dry sample (Zhao et al., 2018), while values in soils are about 10^{10} copies g^{-1} dry sample (Wessén et al., 2010), indicating that bacterial biomass in soils are an order of magnitude higher than in the Heshang cave environment. This site specific work on Heshang cave is consistent with the general observation that fatty acids preserved in speleothems are principally derived from the overlying soil ecosystem and vegetation, having been transported from the surface by percolating groundwater, and with only a minor proportion derived from cave ecosystems (Blyth et al., 2007; Huang et al., 2008; Li et al., 2011; Xie et al., 2005).

Numerous studies have established that, in environmental settings, HMW *n*-fatty acids (C_{20}-C_{32}) with an even number predominance are mainly derived from higher plants (e.g. Eglinton and Hamilton, 1967), whereas LMW *n*-fatty acids (such as C_{16}, C_{18}) are sourced from microbes (Lichtfouse et al., 1995) and higher plants (Chikaraishi and Naraoka, 2006). Hence, this suggests that the HMW *n*-fatty acids in HS4 were primarily derived from higher plants in the overlying catchment, whilst the LMW *n*-fatty acids originated from mixed sources: predominantly microbes in soil-karst system, with some contribution from higher plants. Therefore, changes in the isotopic ratios of stalagmite *n*-fatty acids primarily reflect processes occurring at the subaerial catchment ecosystem above the cave.

Compound-specific isotope analysis is an additional tool to identify the sources of biomarker lipids. For example, significant differences in $\delta^{13}C$ values between the long chain and short chain lipids would indicate they likely originated from different sources (Rieley et al., 1991), because

312 no significant kinetic isotope effect is associated with chain elongation during bacterial fatty acid
313 biosynthesis (Monson and Hayes, 1982), and research shows that the carbon isotope composition
314 of LMW and HMW fatty acids from the same plants are essentially the same (Chikaraishi et al.,
315 2004b). Overall, the strong correlation between $\delta^{13}C_{16FA}$ and $\delta^{13}C_{18FA}$ and between $\delta^{13}C_{22FA}$ and
316 $\delta^{13}C_{24FA}$ (R^2 = 0.79, 0.94, respectively, Fig. 3a, b), and the considerable isotopic differences
317 between the LMW and HMW *n*-fatty acids indicate different biological sources for the LMW and
318 HMW *n*-fatty acids (Figs. 4, 6a)
319
320 *3.4 Holocene vegetation changes derived from $\delta^{13}C_{24FA}$*
321 C_3 plants use the Rubisco enzyme to fix carbon during photosynthesis, which discriminates
322 against the $^{13}CO_2$ isotopologue and therefore results in ^{13}C depletion (relative to C_4 plants). By
323 contrast, C_4 plants (most grasses, sedges and dicots) developed a carbon concentration
324 mechanism during the Miocene (Sage, 2004) that permits them to discriminate less between
325 $^{12}CO_2$ and $^{13}CO_2$; as a result, C_4 plants are more enriched in ^{13}C compared with C_3 plants
326 (Farquhar et al., 1989; Sage, 2004). The resulting isotopic difference between C_3 and C_4 plants is
327 propagated to the *n*-fatty acids they synthesize: typical $\delta^{13}C$ values for *n*-fatty acids from C_3
328 plants range from -30.8‰ to -47.7‰, whilst *n*-fatty acids from C_4 plants range from -16.3‰ to
329 -28.2‰ (Ballentine et al., 1998; Chikaraishi et al., 2004b). Given that CO_2 changes are relatively
330 subtle during the Holocene (changes of ca. 20ppm) (Indermühle et al., 1999), we argue that the
331 general increase in HS4 $\delta^{13}C_{24FA}$ values through the Holocene (Fig. 5a) reflects broad changes in
332 C_3 vs C_4 vegetation in the HS4 catchment.
333 Temperature, precipitation and CO_2 concentrations are the three main controls on C_3/C_4
334 vegetation changes (Ehleringer et al., 1997; Huang et al., 2001). Due to their greater water use
335 efficiency and carbon concentrating mechanism, C_4 plants can theoretically outcompete C_3 plants
336 under conditions of lower pCO_2 and/or higher daytime growing season temperatures (Ehleringer

et al., 1997). However, the dominant control factor may vary spatially and temporally (Huang et al., 2001). Here we expect changes in the $\delta^{13}C$ of the plant wax-derived *n*-C_{24} fatty acid to primarily reflect relative changes in C_3 vs C_4 vegetation driven by changes of temperature and precipitation (Fig. 5a). Our $\delta^{13}C_{24FA}$ data displays a trend towards heavier values that is broadly consistent with the monotonic decline in NH summer insolation (Fig. 5b), along with a general increase in HS4 stalagmite $\delta^{18}O$ (Fig. 5c) which, based on prior work (Cheng et al., 2016), is interpreted to reflect a weakening of the East Asian monsoon during the middle Holocene. The $\delta^{13}C_{24FA}$ trend is also coeval with declining temperatures inferred from the 3-OH-FA based RAN_{15} temperature record from the same stalagmite (Fig. 5d) (Wang et al., 2018), along with changes in hydrology represented by the 3-OH-FA based RIAN proxy (RIAN, the negative logarithm of Branching Ratio; Fig. 5g) (Wang et al., 2018) and dead carbon percentage (DCP, Fig. 5h) (Noronha et al., 2014) from the HS4 speleothem. Noronha et al. (2014) interpret higher DCP to reflect higher precipitation and increased soil moisture, limiting CO_2 diffusion and open-system dissolution, and thus leading to a higher proportion of carbon derived from the ^{14}C-free bedrock.

Closer inspection of our $\delta^{13}C_{24FA}$ record reveals that values are more negative during the HCO (ca. 4.4 to 8.8 ka BP), indicating a greater abundance of C_3 vs. C_4 plants during this relatively wet (Fig. 5c) and warm (Fig. 5d) phase. Following the HCO around ca. 4.4 ka, $\delta^{13}C_{24FA}$ values become more positive, indicating a proportional increase in C_4 vegetation in the Heshang Cave catchment. Critically, the inferred maximum in C_3 abundance at our site during the early Holocene is consistent with maximum expansion of evergreen forest in the middle reaches of the Yangtze River (Sun and Chen, 1991), and is regionally consistent with pollen records from northern China (Ji et al., 2005; Zhou et al., 2010), which show significantly higher percentages of tree pollen during the HCO and a relative decrease in tree pollen during the late Holocene (Fig. 5e-f); the latter shift infers a concomitant increase in grasses and other vegetation types (sedges and dicots), many of which utilise the C_4 pathway. An additional feature of our record worth noting is a rapid excursion to lighter $\delta^{13}C_{24FA}$ values towards the end of the MWP (between ca. 0.6

and 0.8 ka BP), which is again consistent with an increase in tree pollen in Tianchi Lake to the north (Fig. 1, 5f). In light of these phase relationships between regional proxy records in central and northern China, we are confident that temperature and monsoon rainfall were the dominant factors controlling vegetation in the middle reaches of Yangtze River during the Holocene.

3.5 Changes in soil-karst bacterial respiration and substrate selectivity due to Holocene climate change

Holocene variations in $\delta^{13}C$ for the HS4 HMW and LMW *n*-fatty acids are shown in Figure 3a. In contrast to the higher plant derived HMW *n*-fatty acids, the LMW fatty acids are relatively heavier and show more subtle changes in carbon isotope values. Higher plants produce fatty acids with a broad range of chain lengths, characterised by a predominance of HMW even-numbered fatty acids (e.g. C_{24}, C_{26}, C_{28}). However, what is sometimes overlooked is that they also produce shorter chain length compounds (e.g. C_{16}, C_{18}) generally in lower abundances (Chikaraishi et al., 2004b). This means that typically there are no *n*-fatty acids exclusively produced by bacteria preserved in palaeoclimate archives in abundances sufficient for compound-specific isotope analyses. Therefore, in order to constrain bacterial $\delta^{13}C$ signatures we must deconvolve the bacterial $\delta^{13}C$ component from the net $\delta^{13}C$ value (typically some combination of inputs from bacteria, higher plants, and algae) for any given fatty acid.

Unlike in marine or lacustrine systems, algal contributions to the *n*-fatty acid pool in a soil-karst cave system are negligible; thus, the only remaining sources to account for are higher plants and microbes. Archaeal tetra-ether bonded membrane lipids are fundamentally different from bacteria and a negligible source of fatty acids (Koga, 2011). We note that fungi also produce $C_{18:0}$ fatty acid (Zelles, 1997), but the diagnostic biomarker for fungi ($C_{18:2}\omega6,9$) (Frostegård and Bååth, 1996) was found only in trace amounts or not detected at all in our samples, suggesting the contribution of C_{18} fatty acids from fungi is negligible. Thus, we argue that we isolate the first

388 order bacterial contribution to the C_{18} fatty acid, which we term $\delta^{13}C_{18FA(B)}$ (see Section 2.4), and
389 subsequently use this to reconstruct a unique record of Holocene changes in terrestrial bacterial
390 respiration and substrate selectivity. $\delta^{13}C_{18FA(B)}$ varies between -19‰ to -27‰ during the
391 Holocene, becoming generally lighter from 8.5 ka BP (-21‰) to 8 ka BP (-25‰), then heavier to
392 6.1 ka BP (ca. -19‰), lighter to 2.7 ka BP (-27‰), and finally maintaining values of ca. -22‰ to
393 -25‰ with a notable heavy isotope excursion at ca. 0.6 ka BP (-22‰). Superimposed on these
394 broad trends are several single point outliers. Overall, the $\delta^{13}C_{18FA(B)}$ is relatively heavier during
395 the warm/wet phases of the HCO and MWP (Fig. 6b).

396 Soil bacterial respiration is primarily driven by temperature, with a secondary influence of
397 soil moisture (Raich and Tufekciogul, 2000). Warmer climate episodes, such as the HCO and the
398 MWP, are expected to increase rates of bacterial decomposition of soil organic matter (SOM)
399 (Crowther et al., 2016). The stock of SOM in the soil-karst system results from the balance
400 between inputs and outputs of carbon within the belowground environment. Inputs are primarily
401 from leaf and root detritus (including root exudates). Outputs are controlled by the temperature
402 sensitivity of decomposition and leaching. The intrinsic temperature sensitivity of decomposition
403 for a particular soil environment depends on the inventory of the thousands of different organic
404 compounds residing in the soil, each with its own kinetic properties and potential rates of
405 decomposition (Sollins et al., 1996). In most environments, the stocks of labile and recalcitrant
406 compounds are not equal, with recalcitrant compounds being much more abundant than labile
407 compounds (Tjoelker et al., 2001).

408 Modern biogeochemical studies on $\delta^{13}C$ fractionation between SOM substrates and bacterial
409 CO_2 (as a product) help us to interpret our HS4 $\delta^{13}C_{18FA(B)}$ record. A recent synthesis of studies
410 highlights considerable variability, but suggests a ^{13}C enrichment of bacterial CO_2 of up to +5‰
411 compared to the bulk substrate in most cases for C_3 plant dominated soils. Such positive offsets
412 indicate that bacteria preferentially utilise ^{13}C-enriched compounds in the SOM fraction, e.g.
413 sugars, starch, cellulose etc, which are relatively labile (Werth and Kuzyakov, 2010). Šantrůčková

et al. (Šantrůčková et al., 2000) found that the enriching effect associated with the preferential use of organic compounds in C_3 soils is more pronounced than the ^{13}C-depletion effect of metabolism itself. Hence, by preferential substrate utilization in C_3 soils bacterial biomass gets enriched in ^{13}C, but respires CO_2 that is isotopically depleted in ^{13}C relative to bacterial biomass (but still enriched compared to SOM). This effect therefore additionally enriches soil bacteria in ^{13}C (Werth and Kuzyakov, 2010).

Our reconstructed $\delta^{13}C_{18FA(B)}$ in the HCO and MWP portions of our HS4 record are relatively isotopically heavy (Fig. 6). $\delta^{13}C_{18FA(B)}$ also shows a remarkably coherent, anti-phased trend with the carbon isotope values of the acid-soluble organic matter ($\delta^{13}C_{ASOM}$) from the same stalagmite (Fig. 6c) (Li et al., 2014). We interpret this anti-phased trend between $\delta^{13}C_{18FA(B)}$ and $\delta^{13}C_{ASOM}$ record in the HS4 stalagmite as reflecting an increase in substrate selectivity by bacteria of ^{13}C-enriched labile substrates (sugars, starches etc) within the soil organic matter (SOM) pool. This evidence of increased substrate selectivity is intriguing given that the warmer conditions in the HCO and MWP would be conducive to higher rates of soil bacterial activity (Lloyd and Taylor, 1994; Luo, 2007). If inputs from leaf and root detritus and the size of substrate pool remained equal (during the HCO and MWP), we would expect an increase in soil bacterial activity to lead to greater competition for substrates, less selectivity and increased utilization of recalcitrant ^{13}C-depleted substrates (e.g. lipids, wax esters, macro-molecular material etc). However, our results are consistent with increases in gross primary production (GPP) outpacing bacterial respiration (overall increase in net primary production), leading to greater inputs of plant and root detritus, greater selectivity of ^{13}C-enriched labile substrates, and an enriched $\delta^{13}C_{18FA(B)}$ signal. The corollary of this is a greater proportion of recalcitrant ^{13}C-depleted substrates being sequestered in the remaining SOM (Benner et al., 1987; Werth and Kuzyakov, 2010) as represented by the bulk $\delta^{13}C$-ASOM record from HS4 (Li et al., 2014). Our interpretation is consistent with our higher plant $\delta^{13}C$ record (Fig. 5a). We infer the highest proportions of C_3 plant biomass in the HCO and HWP, coeval with our heaviest $\delta^{13}C_{18FA(B)}$ and greatest selectivity of

440 ^{13}C-enriched labile substrates. Preferential substrate utilization is more important in C_3
441 plant-dominated soils because C_4 soils, typical of arid and semiarid climates, contain generally
442 less labile SOM and thus soil bacteria consume the SOM more completely than in C_3 soils
443 (Šantrůčková et al., 2000). This has been demonstrated in modern field studies (see review by
444 Werth and Kuzyakov (2010)) but our reconstruction from HS4 is the first evidence of this
445 relationship on Holocene timescales.

446 To summarize, we argue that because we have isolated the contribution of C_{18} fatty acids
447 from higher plants, the residual $\delta^{13}C$ signal ($\delta^{13}C_{18FA(B)}$) is most parsimoniously explained by
448 greater soil bacterial respiration and decomposition rates, in response to a warmer and wetter
449 local climate, driven by a stronger regional Asian summer monsoon. If net bacterial respiration is
450 substrate-selective, this implies that the more recalcitrant phases are likely escaping heterotrophic
451 degradation. Thus the system acts as a net carbon sink in the early Holocene and would act as a
452 negative feedback on the warmer/wetter local early Holocene climate. This process is likely
453 mediated and enhanced by changes in the relative proportion of C_3 vs C_4 plants. This
454 interpretation of LMW fatty acids is uniquely applicable to speleothems because compared to
455 lake and marine sediments there is minimal contribution from algae, resulting in a simpler two
456 end-member system. This work represents the first such application in a speleothem or indeed
457 any paleoclimate archive. As such, it provides key insights into links between East Asian
458 palaeoclimate, vegetation, terrestrial ecosystem respiration and the carbon cycle during the
459 Holocene.

460

461 **4. Conclusion**

462 We have produced the first reconstruction of vegetation and bacterial activity from the
463 important East Asian monsoon region using compound specific carbon isotopes of fatty acids
464 from a stalagmite. Critically, our study finds that soil bacteria selectively degrade more labile
465 (^{13}C-enriched) substrates during warm periods of the Holocene, suggesting that gross primary

production outpaced soil respiration under higher temperatures. Our findings therefore show that mineral soils in subtropical karst settings may represent a net carbon sink during warmer climate states, thus acting as a negative feedback on Earth's climate.

Acknowledgements

This work was supported by the National Natural Science Foundation of China (Grant Nos. 41807419, 41821001, 41830319, 41773135), the Key R&D Project of Ministry of Science and Technology (grant no. 2016YFA0601100), the 111 project (National Bureau of Foreign Experts and the Ministry of Education of China; Grant No. B08030), and the Fundamental Research Funds for National University, China University of Geosciences, Wuhan (Grant Nos. CUGL170815, CUGCJ1807). We thank the China Scholarship Council (CSC) (Grant No. 201306410031) for supporting Canfa Wang's studies at the University of Birmingham. S.G. was supported by NERC Independent Research Fellowship NE/L011050/1 and NERC large grant NE/P01903X/1 while working on this manuscript. M.L.G. acknowledges support from the National Science Foundation award 1805544. H.Z. acknowledges support from the Hubei Provincial Natural Science Foundation of China (Grant No. 2018CFB398).

References

An, Z., 2000. The history and variability of the East Asian paleomonsoon climate. Quaternary Science Reviews 19, 171-187.

Ballentine, D.C., Macko, S.A., Turekian, V.C., 1998. Variability of stable carbon isotopic compositions in individual fatty acids from combustion of C4 and C3 plants: implications for biomass burning. Chemical Geology 152, 151-161.

Benner, R., Fogel, M.L., Sprague, E.K., Hodson, R.E., 1987. Depletion of ^{13}C in lignin and its implications for stable carbon isotope studies. Nature 329, 708.

Blyth, A.J., Asrat, A., Baker, A., Gulliver, P., Leng, M.J., Genty, D., 2007. A new approach to detecting vegetation and land-use change using high-resolution lipid biomarker records in stalagmites. Quaternary Research 68, 314-324.

Blyth, A.J., Baker, A., Thomas, L.E., Van Calsteren, P., 2011. A 2000-year lipid biomarker record preserved in a stalagmite from north-west Scotland. Journal of Quaternary Science 26, 326-334.

Blyth, A.J., Hartland, A., Baker, A., 2016. Organic proxies in speleothems – New developments, advantages and limitations. Quaternary Science Reviews 149, 1-17.

Blyth, A.J., Smith, C.I., Drysdale, R.N., 2013. A new perspective on the $\delta^{13}C$ signal preserved in speleothems using LC–IRMS analysis of bulk organic matter and compound specific stable isotope analysis. Quaternary Science Reviews 75, 143-149.

Bond-Lamberty, B., Thomson, A., 2010. Temperature-associated increases in the global soil respiration record. Nature 464, 579.

Cheng, H., Edwards, R.L., Sinha, A., Spotl, C., Yi, L., Chen, S., Kelly, M., Kathayat, G., Wang, X., Li, X., Kong, X., Wang, Y., Ning, Y., Zhang, H., 2016. The Asian monsoon over the past 640,000 years and ice age terminations. Nature 534, 640-646.

Chikaraishi, Y., Naraoka, H., 2006. Carbon and hydrogen isotope variation of plant biomarkers in a plant-soil system. Chemical Geology 231, 190-202.

Chikaraishi, Y., Naraoka, H., 2007. $\delta^{13}C$ and δD relationships among three *n*-alkyl compound

508 classes (*n*-alkanoic acid, *n*-alkane and *n*-alkanol) of terrestrial higher plants. Organic
509 Geochemistry 38, 198-215.
510 Chikaraishi, Y., Naraoka, H., Poulson, S.R., 2004a. Carbon and hydrogen isotopic fractionation
511 during lipid biosynthesis in a higher plant (Cryptomeria japonica). Phytochemistry 65, 323-330.
512 Chikaraishi, Y., Naraoka, H., Poulson, S.R., 2004b. Hydrogen and carbon isotopic fractionations
513 of lipid biosynthesis among terrestrial (C_3, C_4 and CAM) and aquatic plants. Phytochemistry 65,
514 1369-1381.
515 Crowther, T.W., Todd-Brown, K.E., Rowe, C.W., Wieder, W.R., Carey, J.C., Machmuller, M.B.,
516 Snoek, B.L., Fang, S., Zhou, G., Allison, S.D., Blair, J.M., Bridgham, S.D., Burton, A.J., Carrillo,
517 Y., Reich, P.B., Clark, J.S., Classen, A.T., Dijkstra, F.A., Elberling, B., Emmett, B.A., Estiarte, M.,
518 Frey, S.D., Guo, J., Harte, J., Jiang, L., Johnson, B.R., Kroel-Dulay, G., Larsen, K.S., Laudon, H.,
519 Lavallee, J.M., Luo, Y., Lupascu, M., Ma, L.N., Marhan, S., Michelsen, A., Mohan, J., Niu, S.,
520 Pendall, E., Penuelas, J., Pfeifer-Meister, L., Poll, C., Reinsch, S., Reynolds, L.L., Schmidt, I.K.,
521 Sistla, S., Sokol, N.W., Templer, P.H., Treseder, K.K., Welker, J.M., Bradford, M.A., 2016.
522 Quantifying global soil carbon losses in response to warming. Nature 540, 104-108.
523 Davidson, E.A., Janssens, I.A., 2006. Temperature sensitivity of soil carbon decomposition and
524 feedbacks to climate change. Nature 440, 165-173.
525 Eglinton, G., Hamilton, R., 1967. Leaf epicuticular waxes. Science 156, 1322.
526 Ehleringer, R.J., Cerling, E.T., Helliker, R.B., 1997. C_4 photosynthesis, atmospheric CO_2, and
527 climate. Oecologia 112, 285-299.
528 Fairchild, I.J., Baker, A., 2012. Speleothem science: from process to past environments. Wiley,
529 Chichester.
530 Farquhar, G.D., Ehleringer, J.R., Hubick, K.T., 1989. Carbon isotope discrimination and
531 photosynthesis. Annual review of plant biology 40, 503-537.
532 Frostegård, Å., Bååth, E., 1996. The use of phospholipid fatty acid analysis to estimate bacterial
533 and fungal biomass in soil. Biology Fertility of Soils 22, 59-65.

534 Genty, D., Blamart, D., Ouahdi, R., Gilmour, M., Baker, A., Jouzel, J., Van-Exter, S., 2003.
535 Precise dating of Dansgaard-Oeschger climate oscillations in western Europe from stalagmite
536 data. Nature 421, 833-837.
537 Hu, C., Henderson, G., Huang, J., Chen, Z., Johnson, K., 2008a. Report of a three-year
538 monitoring programme at Heshang Cave, Central China. International Journal of Speleology 37,
539 143-151.
540 Hu, C., Henderson, G.M., Huang, J., Xie, S., Sun, Y., Johnson, K.R., 2008b. Quantification of
541 Holocene Asian monsoon rainfall from spatially separated cave records. Earth and Planetary
542 Science Letters 266, 221-232.
543 Huang, X., Cui, J., Pu, Y., Huang, J., Blyth, A.J., 2008. Identifying "free" and "bound" lipid
544 fractions in stalagmite samples: An example from Heshang Cave, Southern China. Applied
545 Geochemistry 23, 2589-2595.
546 Huang, Y., Street-Perrott, F.A., Metcalfe, S.E., Brenner, M., Moreland, M., Freeman, K.H., 2001.
547 Climate change as the dominant control on glacial-interglacial variations in C_3 and C_4 plant
548 abundance. Science 293, 1647-1651.
549 Hughen, K.A., Eglinton, T.I., Xu, L., Makou, M., 2004. Abrupt tropical vegetation response to
550 rapid climate changes. Science 304, 1955-1959.
551 Indermühle, A., Stocker, T., Joos, F., Fischer, H., Smith, H., Wahlen, M., Deck, B., Mastroianni,
552 D., Tschumi, J., Blunier, T., 1999. Holocene carbon-cycle dynamics based on CO_2 trapped in ice
553 at Taylor Dome, Antarctica. Nature 398, 121-126.
554 Ji, S., Xingqi, L., Sumin, W., Matsumoto, R., 2005. Palaeoclimatic changes in the Qinghai Lake
555 area during the last 18,000 years. Quaternary International 136, 131-140.
556 Koga, Y., 2011. Early evolution of membrane lipids: how did the lipid divide occur? Journal of
557 Molecular Evolution 72, 274-282.
558 Laskar, J., Robutel, P., Joutel, F., Gastineau, M., Correia, A., Levrard, B., 2004. A long-term
559 numerical solution for the insolation quantities of the Earth. Astronomy and Astrophysics 428,

261-285.

Li, X., Hu, C., Huang, J., Xie, S., Baker, A., 2014. A 9000-year carbon isotopic record of acid-soluble organic matter in a stalagmite from Heshang Cave, central China: Paleoclimate implications. Chemical Geology 388, 71-77.

Li, X., Wang, C., Huang, J., Hu, C., Xie, S., 2011. Seasonal variation of fatty acids from drip water in Heshang Cave, central China. Applied Geochemistry 26, 341-347.

Lichtfouse, É., Berthier, G., Houot, S., Barriuso, E., Bergheaud, V., Vallaeys, T., 1995. Stable carbon isotope evidence for the microbial origin of C_{14}-C_{18} *n*-alkanoic acids in soils. Organic Geochemistry 23, 849-852.

Liu, H., Liu, W., 2017. Concentration and distributions of fatty acids in algae, submerged plants and terrestrial plants from the northeastern Tibetan Plateau. Organic Geochemistry 113, 17-26.

Liu, Q., Wang, H., Zhao, R., Qiu, X., Gong, L., 2010. Bacteria isolated from dripping water in the oligotrophic Heshang cave in central China. Journal of Earth Science 21, 325-328.

Lloyd, J., Taylor, J., 1994. On the temperature dependence of soil respiration. Functional ecology, 315-323.

Luo, Y., 2007. Terrestrial Carbon–Cycle Feedback to Climate Warming. Annual Review of Ecology, Evolution, and Systematics 38, 683-712.

Mahecha, M.D., Reichstein, M., Carvalhais, N., Lasslop, G., Lange, H., Seneviratne, S.I., Vargas, R., Ammann, C., Arain, M.A., Cescatti, A., 2010. Global convergence in the temperature sensitivity of respiration at ecosystem level. Science 329, 838-840.

Matsumoto, G.I., Friedmann, E.I., Watanuki, K., Ocampo-Friedmann, R., 1992. Novel long-chain anteiso-alkanes and anteiso-alkanoic acids in Antarctic rocks colonized by living and fossil cryptoendolithic microorganisms. Journal of Chromatography A 598, 267-276.

Melillo, J.M., Frey, S.D., Deangelis, K.M., Werner, W.J., Bernard, M.J., Bowles, F.P., Pold, G., Knorr, M.A., Grandy, A.S., 2017. Long-term pattern and magnitude of soil carbon feedback to the climate system in a warming world. Science 358, 101-105.

586 Monson, K.D., Hayes, J., 1982. Carbon isotopic fractionation in the biosynthesis of bacterial fatty
587 acids. Ozonolysis of unsaturated fatty acids as a means of determining the intramolecular
588 distribution of carbon isotopes. Geochimica et Cosmochimica Acta 46, 139-149.
589 Noronha, A.L., Johnson, K.R., Hu, C., Ruan, J., Southon, J.R., Ferguson, J.E., 2014. Assessing
590 influences on speleothem dead carbon variability over the Holocene: Implications for
591 speleothem-based radiocarbon calibration. Earth and Planetary Science Letters 394, 20-29.
592 Polissar, P.J., D'Andrea, W.J., 2014. Uncertainty in paleohydrologic reconstructions from
593 molecular δD values. Geochimica et Cosmochimica Acta 129, 146-156.
594 Raich, J.W., Tufekciogul, A., 2000. Vegetation and soil respiration: correlations and controls.
595 Biogeochemistry 48, 71-90.
596 Rieley, G., Collier, R.J., Jones, D.M., Eglinton, G., Eakin, P.A., Fallick, A.E., 1991. Sources of
597 sedimentary lipids deduced from stable carbon-isotope analyses of individual compounds. Nature
598 352, 425.
599 Rubino, M., Etheridge, D., Trudinger, C., Allison, C., Rayner, P., Enting, I., Mulvaney, R., Steele,
600 L., Langenfelds, R., Sturges, W., 2016. Low atmospheric CO_2 levels during the Little Ice Age due
601 to cooling-induced terrestrial uptake. Nature Geoscience 9, 691-694.
602 Sage, R.F., 2004. The evolution of C4 photosynthesis. New phytologist 161, 341-370.
603 Šantrůčková, H., Bird, M., Lloyd, J.J.F.E., 2000. Microbial processes and carbon- isotope
604 fractionation in tropical and temperate grassland soils. Functional Ecology 14, 108-114.
605 Sollins, P., Homann, P., Caldwell, B.A., 1996. Stabilization and destabilization of soil organic
606 matter: mechanisms and controls. Geoderma 74, 65-105.
607 Still, C.J., Berry, J.A., Collatz, G.J., Defries, R.S., 2009. ISLSCP II C4 Vegetation Percentage.
608 ORNL Distributed Active Archive Center.
609 Sun, X., Chen, Y., 1991. Palynological records of the last 11,000 years in China. Quaternary
610 Science Reviews 10, 537-544.
611 Tjoelker, M.G., Oleksyn, J., Reich, P.B., 2001. Modelling respiration of vegetation: evidence for a

612 general temperature- dependent Q_{10}. Global Change Biology 7, 223-230.
613 Wang, C., Bendle, J., Yang, Y., Yang, H., Sun, H., Huang, J., Xie, S., 2016. Impacts of pH and
614 temperature on soil bacterial 3-hydroxy fatty acids: Development of novel terrestrial proxies.
615 Organic Geochemistry 94, 21-31.
616 Wang, C., Bendle, J.A., Zhang, H., Yang, Y., Liu, D., Huang, J., Cui, J., Xie, S., 2018. Holocene
617 temperature and hydrological changes reconstructed by bacterial 3-hydroxy fatty acids in a
618 stalagmite from central China. Quaternary Science Reviews 192, 97-105.
619 Wang, C., Zhang, H., Huang, X., Huang, J., Xie, S., 2012. Optimization of acid digestion
620 conditions on the extraction of fatty acids from stalagmites. Frontiers of Earth Science 6,
621 109-114.
622 Wang, Z., Liu, W.G., 2012. Carbon chain length distribution in n-alkyl lipids: A process for
623 evaluating source inputs to Lake Qinghai. Organic Geochemistry 50, 36-43.
624 Werth, M., Kuzyakov, Y., 2010. ^{13}C fractionation at the root–microorganisms–soil interface: a
625 review and outlook for partitioning studies. Soil Biology and Biochemistry 42, 1372-1384.
626 Wessén, E., Hallin, S., Philippot, L., 2010. Differential responses of bacterial and archaeal groups
627 at high taxonomical ranks to soil management. Soil Biology and Biochemistry 42, 1759-1765.
628 Xie, S., Evershed, R.P., Huang, X., Zhu, Z., Pancost, R.D., Meyers, P.A., Gong, L., Hu, C., Huang,
629 J., Zhang, S., 2013. Concordant monsoon-driven postglacial hydrological changes in peat and
630 stalagmite records and their impacts on prehistoric cultures in central China. Geology 41,
631 827-830.
632 Xie, S., Huang, J., Wang, H., Yi, Y., Hu, C., Cai, Y., Cheng, H., 2005. Distributions of fatty acids
633 in a stalagmite related to paleoclimate change at Qingjiang in Hubei, southern China. Science in
634 China Series D: Earth Sciences 48, 1463-1469.
635 Xie, S., Yi, Y., Huang, J., Hu, C., Cai, Y., Collins, M., Baker, A., 2003. Lipid distribution in a
636 subtropical southern China stalagmite as a record of soil ecosystem response to paleoclimate
637 change. Quaternary Research 60, 340-347.

638 Yun, Y., Xiang, X., Wang, H., Man, B., Gong, L., Liu, Q., Dong, Q., Wang, R., 2016. Five-year
639 monitoring of bacterial communities in dripping water from the Heshang Cave in central China:
640 Implication for paleoclimate reconstruction and ecological functions. Geomicrobiology Journal
641 33, 553-563.
642 Zelles, L., 1997. Phospholipid fatty acid profiles in selected members of soil microbial
643 communities. Chemosphere 35, 275-294.
644 Zhang, Z., Zhao, M., Eglinton, G., Lu, H., Huang, C.-Y., 2006. Leaf wax lipids as
645 paleovegetational and paleoenvironmental proxies for the Chinese Loess Plateau over the last 170
646 kyr. Quaternary Science Reviews 25, 575-594.
647 Zhao, R., Wang, H., Cheng, X., Yun, Y., Qiu, X., 2018. Upland soil cluster γ dominates the
648 methanotroph communities in the karst Heshang Cave. FEMS Microbiology Ecology 94, fiy192.
649 Zhou, A., Sun, H., Chen, F., Zhao, Y., An, C., Dong, G., Wang, Z., Chen, J., 2010. High-resolution
650 climate change in mid-late Holocene on Tianchi Lake, Liupan Mountain in the Loess Plateau in
651 central China and its significance. Chinese Science Bulletin 55, 2118-2121.
652 Zhu, Z., Feinberg, J.M., Xie, S., Bourne, M.D., Huang, C., Hu, C., Cheng, H., 2017. Holocene
653 ENSO-related cyclic storms recorded by magnetic minerals in speleothems of central China.
654 Proceedings of the National Academy of Sciences of the United States of America 114, 852-857.
655
656

Figure Captions

Fig. 1. Location of Heshang Cave, Qinghai Lake and Tianchi Lake. The distribution of C_4 vegetation in Asia is after Still et al. (2009). The inset is map shows the main regional surface drainage and location of Heshang cave on the Qing River tributary of the Yangtze (revised after Hu et al. (2008a)).

Fig. 2. Distribution and relative abundance of fatty acids in (a, b) cave overlying soil, and (c, d) HS4 stalagmite. "*i*-" refers to "*iso*", "*a*-" refers to "*anteiso*" and "*n*-" refers to "*normal*". *n*-C_{16} fatty acid is dominant in low molecular weight fatty acids($\leq C_{20}$), *n*-C_{24} fatty acid is dominant in high molecular weight fatty acids ($>C_{20}$).

Fig. 3. Plots showing the relationship between $\delta^{13}C$ values of *n*-fatty acids from HS4 stalagmite. **a**, Linear correlation between $\delta^{13}C_{16FA}$ and $\delta^{13}C_{18FA}$ based on a data set of 70 samples ($R^2 = 0.79$, $p < 0.001$). **b**, Linear correlation between $\delta^{13}C_{16FA}$ and $\delta^{13}C_{24FA}$ based on a data set of 61 samples ($R^2 = 0.55$, $p < 0.001$). **c,** Linear correlation between $\delta^{13}C_{22FA}$ and $\delta^{13}C_{24FA}$, based on a data set of 49 samples ($R^2 = 0.94$, $p < 0.001$). **d**, Linear correlation between $\delta^{13}C_{18FA}$ and $\delta^{13}C_{24FA}$ based on a data set of 59 samples ($R^2 = 0.61$, $p < 0.001$).

Fig. 4. Box chart showing the carbon isotope values of C_{16}, C_{18}, C_{22} and C_{24} *normal* (*n*-) fatty acids (FAs) from HS4 stalagmite.

Fig. 5. Vegetation changes and climatic drivers in central China during the last 9 ka BP. **a**, Variation of $\delta^{13}C_{24FA}$ showing vegetation changes during the last 9 ka BP. **b**, Insolation changes at 30°N in July during the last 9 ka BP (Laskar et al., 2004). **c**, Calcite $\delta^{18}O$ of HS4 stalagmite over the past 9 ka BP (Hu et al., 2008b). **d**, Temperature variation during the last 9 ka BP

683 reconstructed by ratio of *anteiso* to *normal* C_{15} 3-hydroxy fatty acid (RAN_{15}; temperature proxy)
684 from HS4 stalagmite from Heshang Cave, central China (Wang et al., 2018). **e**, Percentage of tree
685 pollen from Qinghai Lake sediment (Ji et al., 2005). **f**, Percentage of deciduous tree pollen from
686 Tianchi Lake (Zhou et al., 2010). **g,** Heshang Cave hydrological conditions inferred from the
687 RIAN proxy (RIAN, the negative logarithm of Branching Ratio) from HS4 stalagmite during the
688 last 9 ka BP (Wang et al., 2018). **h**, Dead carbon proportion (DCP) from HS4 stalagmite
689 (Noronha et al., 2014). Blue shading highlights two periods with relative low percentage of C_3
690 plants during the HCO. Orange shading highlights relatively high percentages of C_3 plants during
691 the HCO and MWP. Black line segments showing the U-Th dating errors.
692
693 **Fig. 6.** Vegetation changes and soil bacterial heterotrophic selectivity and respiration rates in
694 response to climate changes. **a**, Compound specific $\delta^{13}C$ values measured on the *n*-C_{16}, *n*-C_{18},
695 *n*-C_{22}, *n*-C_{24} fatty acids extracted from the HS4 stalagmite. **b**, Variation in $\delta^{13}C_{18FA(B)}$ over the last
696 9 ka BP with locally weighted scatterplot smoothing of 25% (LOWESS). **c**, Acid-soluble organic
697 matter (ASOM) carbon isotope ($\delta^{13}C_{ASOM}$) sequence derived from HS4 stalagmite (grey line) and
698 three-point running average (red line) (Li et al., 2014). **d**, Temperature variation during the last 9
699 ka BP reconstructed by RAN_{15} from HS4 stalagmite from Heshang Cave, central China (Wang et
700 al., 2018). **e**, Calcite $\delta^{18}O$ of HS4 stalagmite over the past 9 ka BP (Hu et al., 2008b). U-Th dating
701 errors (Hu et al., 2008b) are shown as black line segments.

Figure 1

Click here to download high resolution image

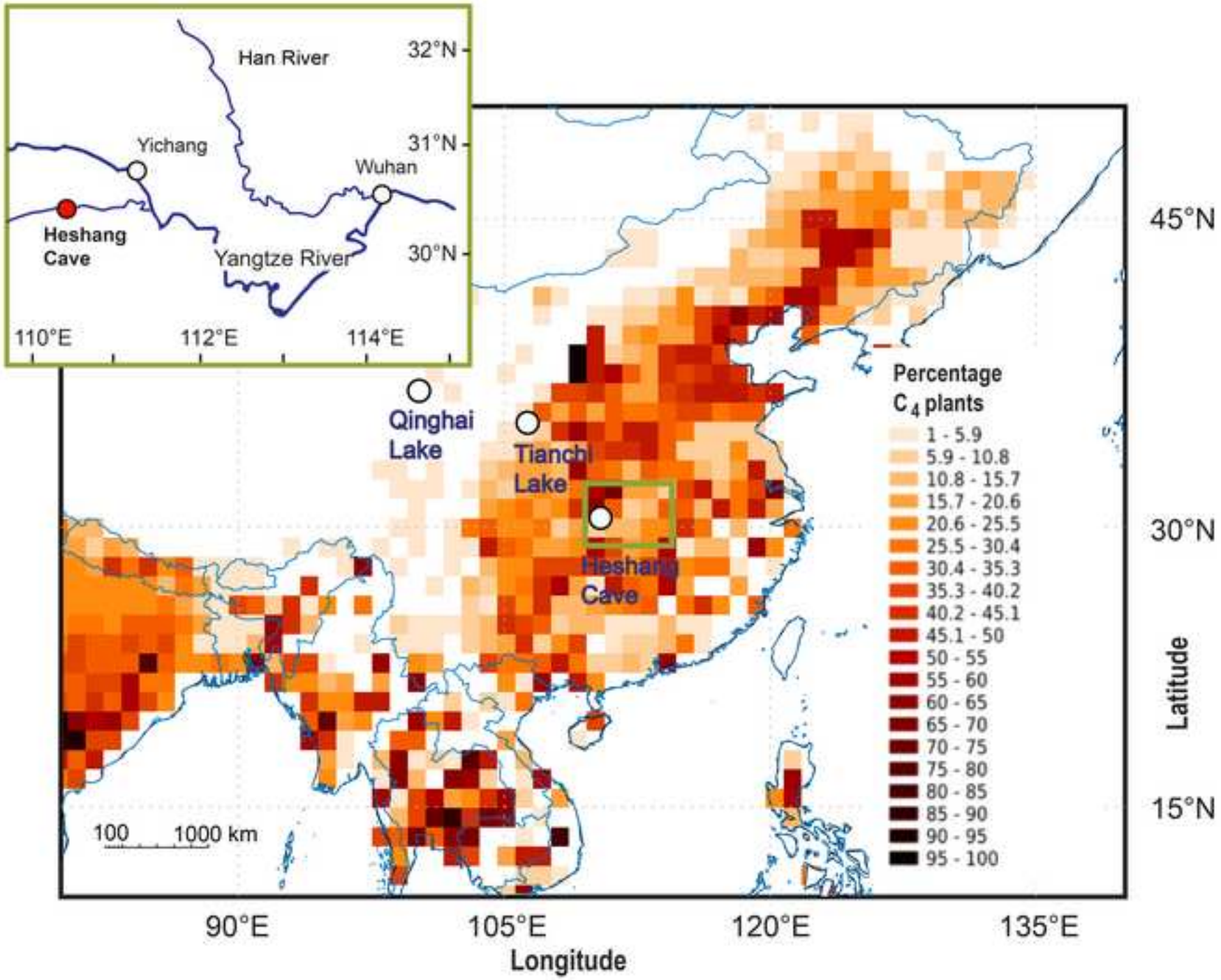

Figure 2

Click here to download high resolution image

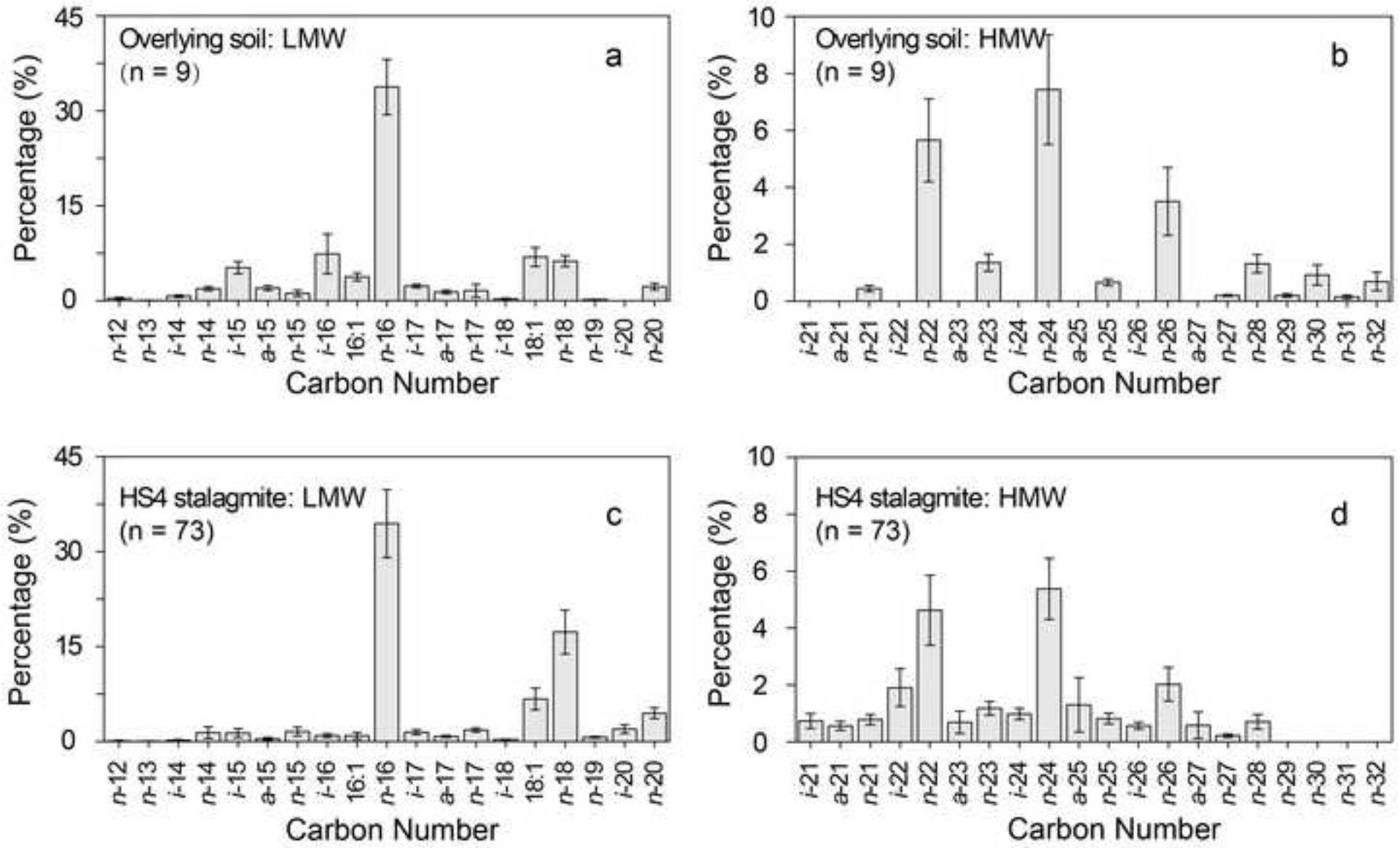

Figure 3

Click here to download high resolution image

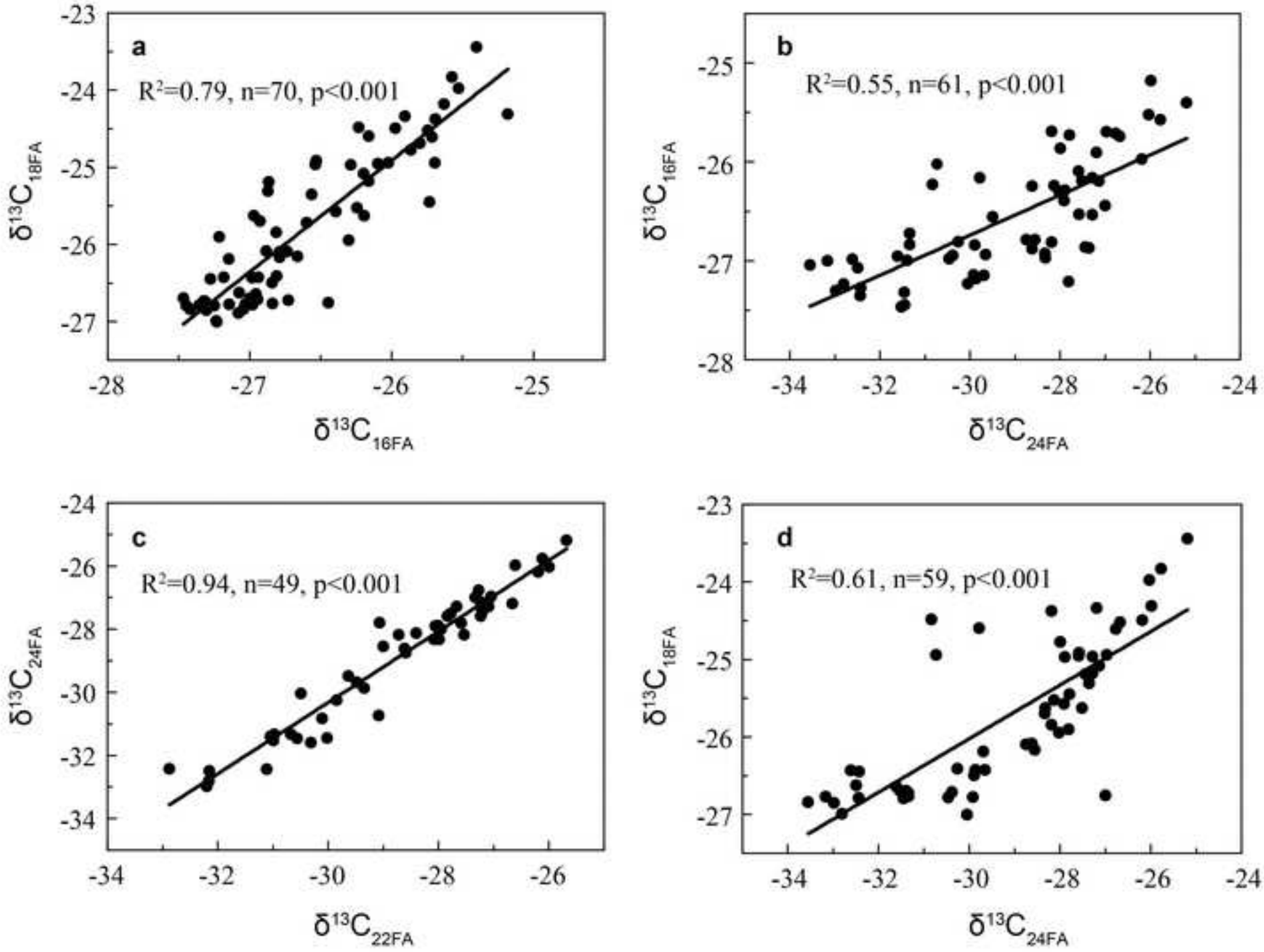

Figure 4

Click here to download high resolution image

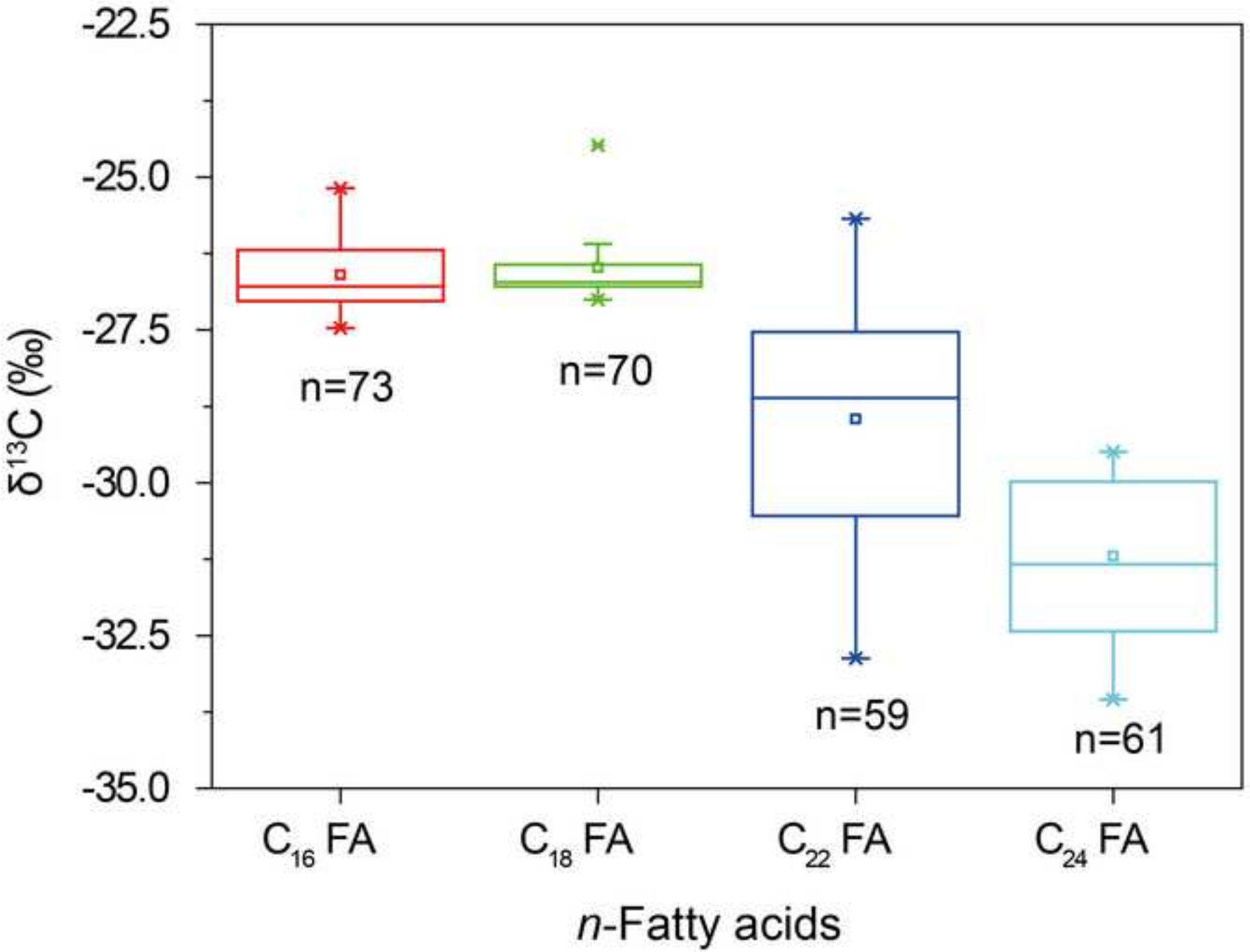

Figure 5

Click here to download high resolution image

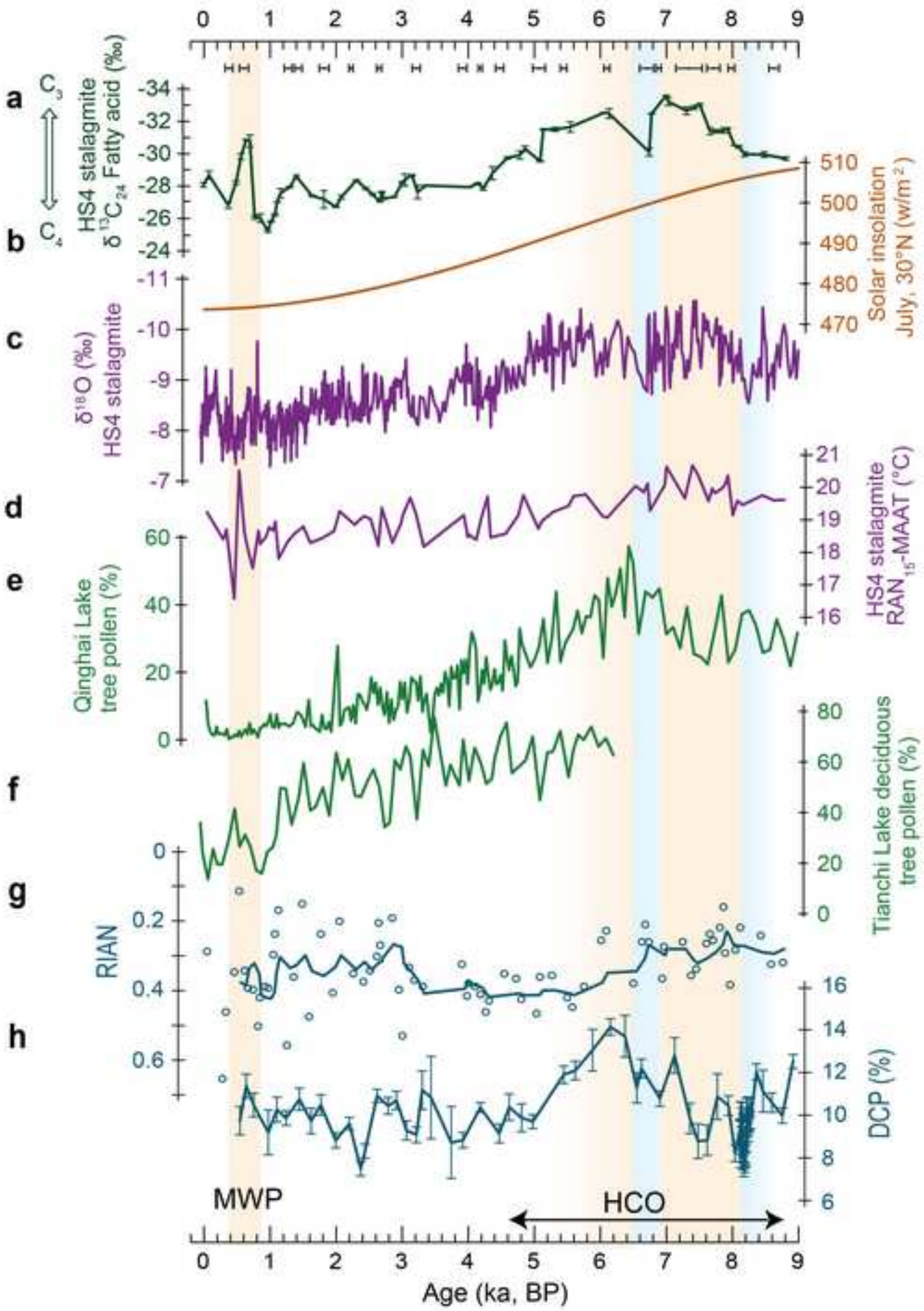

Figure 6

Click here to download high resolution image

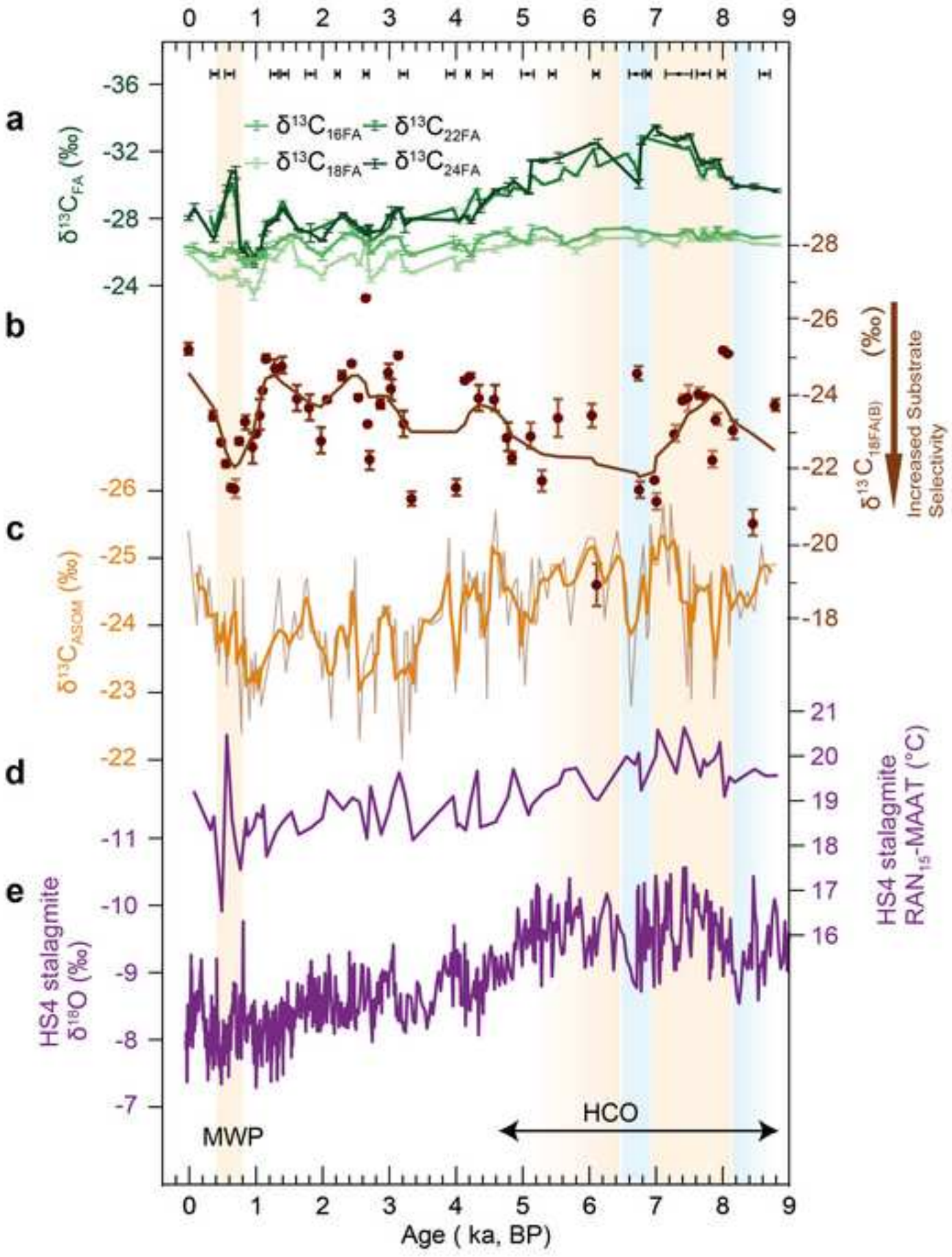

Figure 1 (high-resolution)

Click here to download Figure (high-resolution): Figure 1.tif

Figure 2 (high-resolution)

Click here to download Figure (high-resolution): Figure 2.tif

Figure 3 (high-resolution)

Click here to download Figure (high-resolution): Figure 3.tif

Figure 4 (high-resolution)

Click here to download Figure (high-resolution): Figure 4.tif

Figure 5 (high-resolution)

Click here to download Figure (high-resolution): Figure 5.tif

Figure 6 (high-resolution)

Click here to download Figure (high-resolution): Figure 6.tif

Supplementary material for online publication only

Click here to download Supplementary material for online publication only: Supplementary Information.docx